Applied Catalysis B: Environmental 180 (2016) 674–679

Contents lists available at ScienceDirect

Applied Catalysis B: Environmental

journal homepage: www.elsevier.com/locate/apcatb

Anion exchange membrane water electrolyzer with an ultra-low loading of Pt-decorated Ni electrocatalyst

Sang Hyun Ahn[a,b], Sung Jong Yoo[a], Hyoung-Juhn Kim[a], Dirk Henkensmeier[a], Suk Woo Nam[a,d], Soo-Kil Kim[c,**], Jong Hyun Jang[a,d,*]

[a] Fuel Cell Research Center, Korea Institute of Science and Technology (KIST), Hwarangno 14-gil 5, Seongbuk-gu, Seoul 136-791, Republic of Korea
[b] School of Chemical Engineering and Materials Science, Chung-Ang University, Heukseokno 84, Dongjak-gu, Seoul 156-756, Republic of Korea
[c] School of Integrative Engineering, Chung-Ang University, Heukseokno 84, Dongjak-gu, Seoul 156-756, Republic of Korea
[d] Green School, Korea University, Anam-ro 145, Seongbuk-gu, Seoul 136-713, Republic of Korea

ARTICLE INFO

Article history:
Received 17 May 2015
Accepted 14 July 2015
Available online 19 July 2015

Keywords:
Anion exchange membrane water electrolyzer
Hydrogen evolution reaction
Pt-decorated Ni electrocatalyst
Ultra-low Pt loading

ABSTRACT

The particle-type electrodes with ultra-low electrocatalyst loading (<10 μg cm^{-2}) were developed as cathodes in the anion exchange membrane water electrolyzer (AEMWE). The Pt-decorated Ni electrocatalysts were prepared on the surface of carbon paper by Ni electrodeposition and subsequent displacement of Ni by Pt; the composition and morphology were controlled by varying HCl concentration. In half cell test, the increase of hydrogen evolution reaction (HER) activity by Pt decoration was confirmed for Pt-Ni/CP-2 that has Pt ratio of 39.4% (1.85 μg$_{Pt}$ cm^{-2}). A membrane electrode assembly employing Pt-Ni/CP-2 as the HER electrode (total catalyst loading: 13.2 μg cm^{-2}) exhibited a current density of 250 mA cm^{-2} at 1.9 V$_{cell}$ (50 °C), which is comparable to the previous reports with much larger loading of 3.1 ~ 80 mg cm^{-2}.

1. Introduction

Water electrolysis has been recognized as a promising technique to produce hydrogen through environmentally friendly processes associated with renewable electricity sources, such as solar and wind [1]. As electrolytes in water electrolysis cells, alkaline liquids with diaphragm separators have been widely developed and utilized [2]. However, recently, the solid polymer electrolyte water electrolyzer (SPEWE) technique has received a great deal of attention. This technique has several advantages because its compact design enables high efficiency, hydrogen production rate, and hydrogen purity, as well as allowing high-pressure operation [3–5]. For SPEWEs, two types of solid polymer electrolyte have mainly been investigated: proton exchange membranes [3,4] and anion exchange membranes [5]. The proton exchange membrane water electrolyzer (PEMWE) has been considered to be a strong candidate for providing an effective method of hydrogen production because their well-developed solid polymer electrolyte and ionomer (e.g. Nafion) facilitate a higher hydrogen production rate compared to the anion exchange membrane water electrolyzer (AEMWE) [3,4]. However, the severe acidic conditions present in PEMWEs makes their commercialization costly because of the need to use noble metal catalysts for both the cathode and anode (about 2 ~ 4 mg cm^{-2}) [6]. Pt is generally employed as an electrocatalyst for the hydrogen evolution reaction (HER) at the cathode, though other platinum-group-metals (PGM), such as Ir and Pd, are also under investigation [6,7]. Precious metal oxides (e.g. RuO_2 and IrO_2) and their admixtures are conventionally used for the oxygen evolution reaction (OER) at the anode, due to their high activity and stability [8,9]. In addition, the harsh oxidative environment present in PEMWEs demands not only noble metal catalysts but also high-priced components such as Ti-based current collectors and separators [10]. On the other hand, non-noble catalysts can also be used for both the HER and OER electrode in AEMWEs [2,5].

For membrane electrode assembly (MEA) fabrication, conventional porous electrodes have generally been employed, where a catalyst powder is mixed with a binder and coated onto the membrane or gas diffusion layer (GDL) [11–19]. Typically, this kind of electrode has a thickness of several micro-meters with a metal loading of the order of milligrams. For example, Scott et al. reported the performance of AEMWEs using various Co-based oxides (2.5–3.0 mg cm^{-2}) and Ni (2.0 mg cm^{-2}) as the OER

* Corresponding author at: Fuel Cell Research Center, Korea Institute of Science and Technology (KIST), Hwarangno 14-gil 5, Seongbuk-gu, Seoul 136-791, Republic of Korea. Fax: +82 2 958 5199.
** Corresponding author at: School of Integrative Engineering, Chung-Ang University, Heukseokno 84, Dongjak-gu, Seoul 156-756, Republic of Korea. Fax: +82 2 814 2651.
E-mail addresses: sookilkim@cau.ac.kr (S.-K. Kim), jhjang@kist.re.kr (J.H. Jang).

http://dx.doi.org/10.1016/j.apcatb.2015.07.020
0926-3373/

and HER catalysts, respectively [11–13,16,17]. The current densities reported at a cell voltage of 1.9 V ranged from 65 mA cm^{-2} (3.0 mg cm^{-2} of $Cu_{0.7}Co_{2.3}O_4$) [11] to 175 mA cm^{-2} (2.5 mg cm^{-2} of Li-doped Co_3O_4) [13]. Comotti et al. demonstrated the effect of HER catalyst (Ni/(CeO_2-La_2O_3)/C) loading on AEMWE performance, where, as the loading varied from 0.6 to 7.4 mg cm^{-2}, the current density at 1.9 V increased from 160 to 470 mA cm^{-2} [14]. Xiao et al. reported an enhanced AEMWE performance of 570 mA cm^{-2} at 1.9 V using extremely high catalyst loadings for both the HER (Ni-Mo: 40 mg cm^{-2}) and OER (Ni-Fe: 40 mg cm^{-2}) electrodes [15]. This performance is comparable to that observed using PGM and oxide catalysts for the HER (Pt, 3.2 mg cm^{-2}) and OER (IrO_2, 2.9 mg cm^{-2}) electrodes, respectively [19].

Although the use of huge amounts of non-noble catalysts facilitates reasonable cell performance, the thicker catalyst layer required is expected to encounter severe reactant/product transport difficulties and low catalyst utilization. Particularly, the large ohmic drop at these gas-evolving electrodes induced by hydrogen and oxygen bubbles trapped in the catalyst layer and GDL pores will become increasingly significant at higher current densities. In evidence of this, Bazylak et al. exhibited images of bubbles trapped inside three types of GDL (foam, felt, and sintered powder), the presence of which depended on the GDL porosity [20]. These results show that the significance of trapped bubbles in the GDL becomes more severe when the GDL porosity is lower. Zhang et al. also demonstrated the significance of the bubble ohmic drop through a comparison of stagnant and flow cells [21]. The current loss induced by trapped bubbles was relieved by pushing the bubbles out of the cell with a continuous flow of reactant. Another challenge related to using a thick catalyst layer with a high metal loading is low catalyst utilization. This originates from the low ionic conductivity of the hydroxide-conducting ionomer used in the present technology, although methods to improve ionic conductivity are under extensive investigation [5,22]. In addition, the cost associated with using high catalyst loadings should also be considered, even though non-noble metals are lower-priced than PGM.

Alternatively to conventional porous electrodes, particle-type electrodes produced through the direct formation of catalysts on the surface of GDLs are expected to provide facile transport and high catalyst utilization. For AEMWEs, we previously reported particle-type electrodes fabricated by Ni electrodeposition on carbon paper (CP) fibers [23]. The performance of our cell was 150 mA cm^{-2} at 1.9 V despite the extremely small amount of Ni nanoparticle catalyst present (8.51 μg_{Ni} cm^{-2}). The relatively high performance of our cell was probably due to minimized ohmic resistance, high catalyst utilization, and rapid transportation. Additionally, electrodeposition has its own merits as an electrode fabrication method because it is a simple process with short process time. However, the lack of active sites created from small loadings still limits cell performance and restricts their practical application.

In the present study, in order to increase the performance of particle-type electrodes, we demonstrate an electrochemical modification of the electrodeposited Ni nanoparticles through Ni displacement by Pt. While maintaining the extremely small catalyst loadings and the merits derived from this, a simple displacement of the Ni surface with Pt is expected to significantly increase cell performance due to the intrinsically high HER activity of Pt in alkaline electrolytes [24]. The effect of changes in morphology and composition of the Pt decorated Ni particles as well as the synergetic effect between Ni and Pt on HER activity are discussed.

2. Experimental

The Ni/CP electrodes were prepared according to the procedure described in our previous report [23]. The Ni electrodeposition was carried out on the CP (TGPH-090, Toray) in 0.5 M $NiCl_2$ solution (pH 2.5) at −0.95 V_{SCE} for 50 s. The Ni/CP electrodes were immersed in the solutions containing 1 mM K_2PtCl_6 (Sigma–Aldrich) with various HCl concentration (10, 50, and 100 mM) for 180 s, in order to fabricate Pt-Ni/CP electrodes through galvanic displacement of Pt on Ni/CP.

The prepared Pt-Ni/CP electrodes were chracterized by microscopic and spectroscopic techniques. The morphological changes after Pt galvanic displacement were observed by field emission scanning electron microscope (FESEM, S-4100, Hitachi) and electron probe micro analyzer (EPMA; JXA-8500F, JEOL). The Pt and Ni loading mass of Ni/CP and Pt-Ni/CP electrodes were anlayzed by inductively coupled plasma mass spectrometry (ICPMS, ELAN 6100 DRC Plus, PerkinElmer SCIEX). The electronic structures of Ni/CP and Pt-Ni/CP electrode were analyzed by X-ray photoelectron spectroscopy (XPS; PHI 5800 ESCA).

For electrochemical analysis, a conventional three electrodes cell system was used with Pt sputtered Ti mesh and a saturated calomel electrode (SCE, Sigma–Aldrich) as a counter and a reference electrodes, respectively. As working electrodes, Ni/CP and Pt-Ni/CP were placed in a home-made Teflon® holder to expose designated area (10.24 cm^2) of samples to electrolytes. All of electrochemical analysis was controlled by potentiostat (Autolab PGSTAT302, Metrohm). For catalyic activity test toward HER and OER, cyclic voltammetry was carried out in 1.0 M KOH aqueous solution with a scan rate of 50 mV s^{-1} at room temperature. Prior to every electrochemical measurement, electrolytes were purged to eliminate the dissoluved oxygen by nitrogen gas with a flow rate of 50 cm^3 min^{-1} for 10 min. The measured potentials with SCE were converted to reversible hydrogen electrode (RHE).

To evaluate the AEMWE performances, a single cell was fabricated by combining commercial anion exchange membrane (A201, Tokuyama), electrodes, and graphite bipolar plates. For HER, Pt-Ni/CP electrode was employed, whereas the Ni/CP electrode was used for OER. The compression pressure of membrane electrode assembly (MEA, 2 × 2 cm^2) by end plates was 4.1 MPa. The cell performance was observed under constant current density controlled by a potentiostat (HCP 803, Bio-logic). The cell temperature was fixed to 50 °C and 70 °C by external electric power. The reactant of 1.0 M KOH was pre-heated to 50 °C and injected into cathode (HER) with feed rate of 1 mL min^{-1} by using syringe pump (KDS100, KD Scientific).

3. Results and discussion

Fig. 1(a) displays a field emission scanning electron microscopy (FESEM) image of the Ni/CP electrodes prepared by electrodeposition at a deposition potential of −0.95 V_{SCE} for 50 s [23]. The Ni nanoparticles were observed to have superficial dendritic shapes with large populations present on the surface of the CP fibers that will provide a number of reaction sites. Ni displacement by Pt was conducted on the Ni/CP electrodes in 1 mM K_2PtCl_6 solution with varying HCl concentrations (10 ~ 100 mM) for 180 s. With 10 mM HCl, spherical dots (diameter: ~120 nm) were sparsely formed on the Ni nanoparticle surface (Pt-Ni/CP-1, Fig. 1b). As the HCl concentration increased to 50 mM (Pt-Ni/CP-2, Fig. 1c), the Ni nanoparticle surface became highly populated with dots (diameter ~50 nm). As the HCl concentration was further increased to 100 mM, the Pt coverage increased again while the size of the dots decreased, as shown in Fig. 1d (Pt-Ni/CP-3). It is also noted that the Ni coverage of CP continuously decreased with increasing HCl concentration due to severe dissolution of Ni. As confirmed by the FESEM images, the morphology of the Pt-Ni particles depended significantly on the HCl concentration.

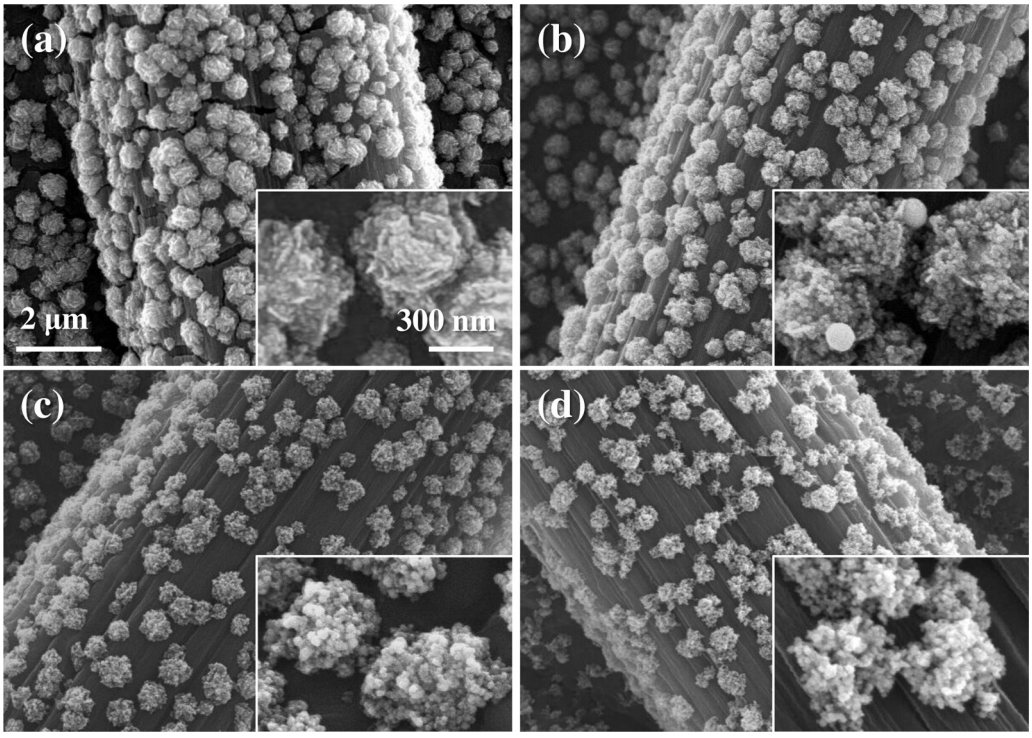

Fig. 1. FESEM images of the (a) Ni/CP, (b) Pt-Ni/CP-1, (c) Pt-Ni/CP-2, and (d) Pt-Ni/CP-3 electrodes. Insets: enlarged images.

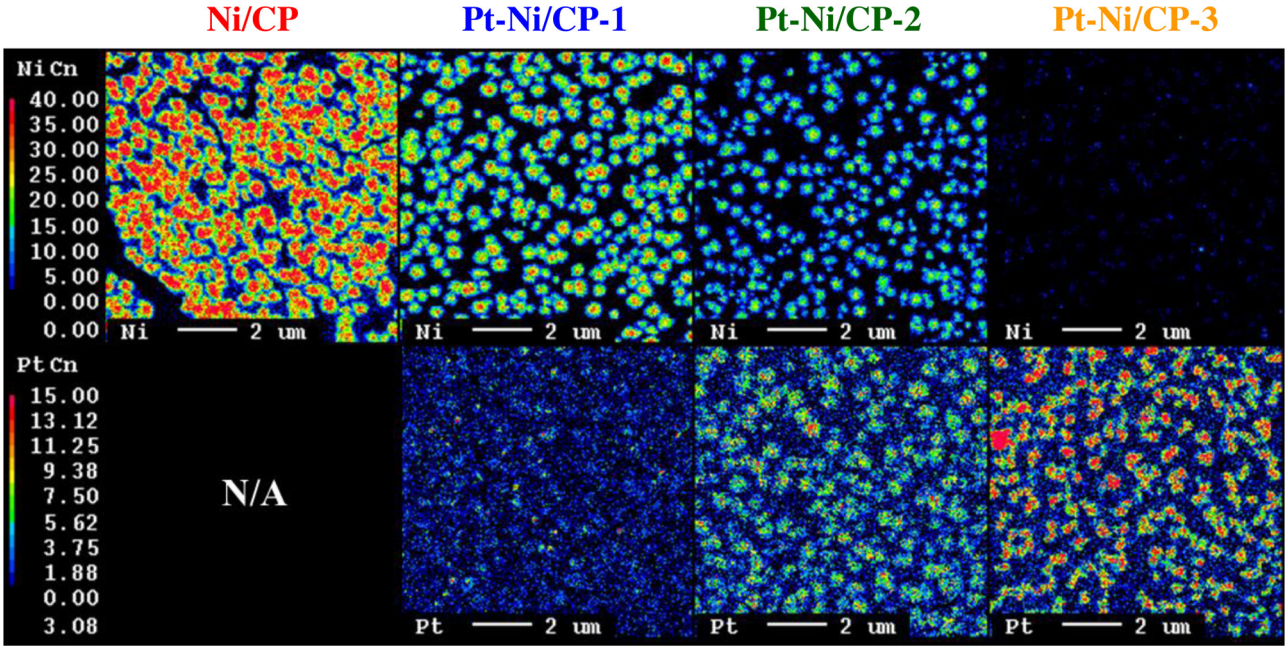

Fig. 2. EPMA mapping of the Ni/CP and Pt-Ni/CP electrodes (top images for Ni and bottom images for Pt).

Compositional changes were also confirmed by electron probe micro analyzer (EPMA) mapping as illustrated in Fig. 2. The Ni content and coverage gradually decreased with increasing HCl concentration (top images, left to right, Ni/CP → Pt-Ni/CP-3). In the case of the Pt content (bottom images, left to right), the Pt dots were only sparsely found in the image of Pt-Ni/CP-1, and subsequently Pt became well dispersed with increasing HCl concentration. Particularly for Pt-Ni/CP-2, the Pt positions were in excellent agreement with the remaining Ni sites indicating that Pt selectively decorated the Ni surface. The Ni particles were severely dissolved and entirely displaced (or covered) with Pt if the HCl concentration was increased further (Pt-Ni/CP-3). These EPMA results also successfully support the above description of the morphology changes observed by FESEM.

Fig. 3a and b show enlarged images of the EPMA mapping of a single Pt-Ni particle of Pt-Ni/CP-2. The atomic signals of Pt were well matched with that of the Ni boundary. Comparison of the line profiles shown in Fig. 3c indicated that the Pt particles were effectively covering the underlying Ni particles (denoted as Pt-decorated Ni). This is similar to the core-shell particle [25] though the parti-

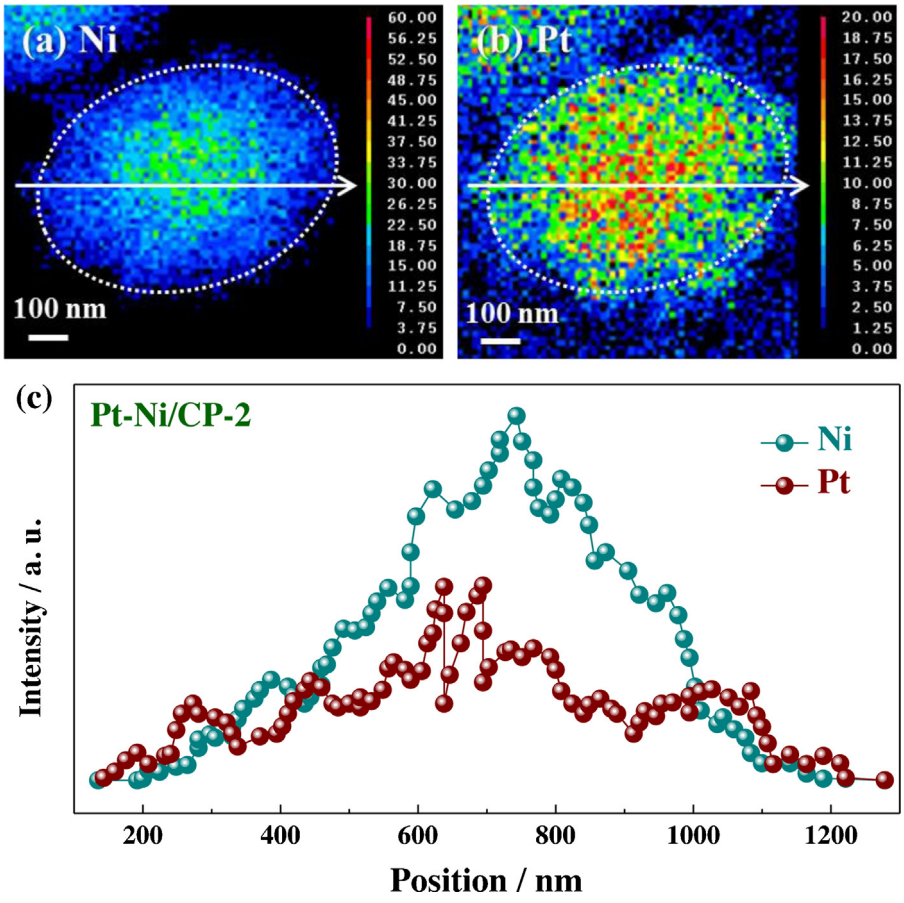

Fig. 3. Enlarged image of EPMA mapping for a single Pt-Ni particle on the Pt-Ni/CP-2 electrode for (a) Ni and (b) Pt. (c) Elemental line scanning of Ni and Pt following the white arrow in Fig. 3(a) and (b).

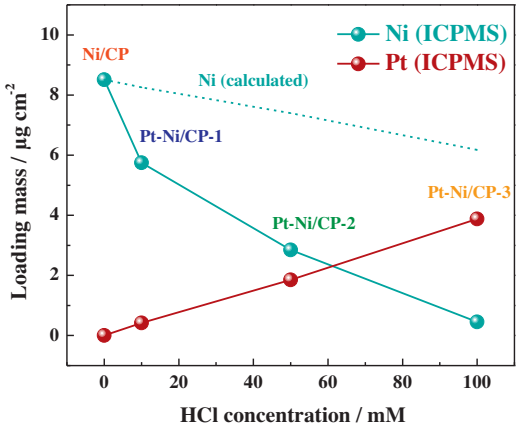

Fig. 4. Measured Pt and Ni loading mass of Ni/CP and Pt-Ni/CP electrodes as a function of HCl concentration in Pt displacement solution (solid line). Calculated Ni loading mass based on measured Pt loading mass (dot line).

cles present on our Pt-Ni/CP electrode were about hundred times larger.

Fig. 4 shows the dependence of Pt and Ni loading on the HCl concentration in the displacement solution. As the HCl concentration increased, the Pt loading linearly increased from 0 to 3.88 μg_{Pt} cm_{geo}^{-2}, whereas the Ni loading decreased from 8.51 to 0.45 μg_{Ni} cm_{geo}^{-2}. As a result, the Pt weight ratio gradually increased as 6.8 % (Pt-Ni/CP-1) → 39.4% (Pt-Ni/CP-2) → 89.6% (Pt-Ni/CP-3). At the Ni surface, the spontaneous displacement of Ni by Pt was carried out as shown below (Ni^{2+}/Ni: −0.257 V_{SHE} and $PtCl_6^{2-}$/Pt: 0.744 V_{SHE}) [26]:

$$3Ni/CP + PtCl_6^{2-} \rightarrow Pt - Ni/CP + 2Ni^{2+} + 6Cl^{-} \quad (1)$$

Based on the measured Pt loadings, theoretical Ni loadings were calculated using the displacement reaction stoichiometry (Eq. (1)), and then compared with the measured Ni loadings. As the HCl concentration increased, the gap between the measured and calculated Ni loadings widened from 2.51 to 5.73 μg_{Ni} cm_{geo}^{-2}. Evidently, the coverage of Pt-Ni nanoparticles on the surface of CP fibers decreased notably with increasing HCl concentration (Figs. 1 and 2), supporting the premise that the surface exchange of Ni by Pt is a slower process than the dissolution of uncovered Ni as also reported by Sotiropoulos and his colleagues [26]. Fig. 4 also shows that that the synergistic effects from the interface of Pt and Ni was expectable in the case of Pt-Ni/CP-2, while Pt-Ni/CP-3 seems to be more like to Pt/CP due to the severe dissolution.

Fig. 5 demonstrates the XPS analysis on the Ni/CP and Pt-Ni/CP electrodes. For Ni $2p_{3/2}$ and Ni 3p spectra, the intensity was monotonically decreased by increase of HCl concentration in Pt displacement solution (red → orange), whereas the intensity of Pt 4f spectra appeared and then increased (Fig. 5b). The quantitative calculation of XPS spectra area indicated the Pt molar concentration of 7.8% for Pt-Ni/CP-1 and 63.6% for Pt-Ni/CP-2, respectively, which were larger than Pt molar concentrations for Pt-Ni/CP-1 (2.1%) and Pt-Ni/CP-2 (16.4 %) obtained by ICPMS. This also confirmed the Pt decoration at the surface of Ni after the displacement. For Pt-Ni/CP-3, the both of Ni $2p_{3/2}$ and 3p XPS spectra was not detected demonstrating that the most of particle surface was consisted of Pt,

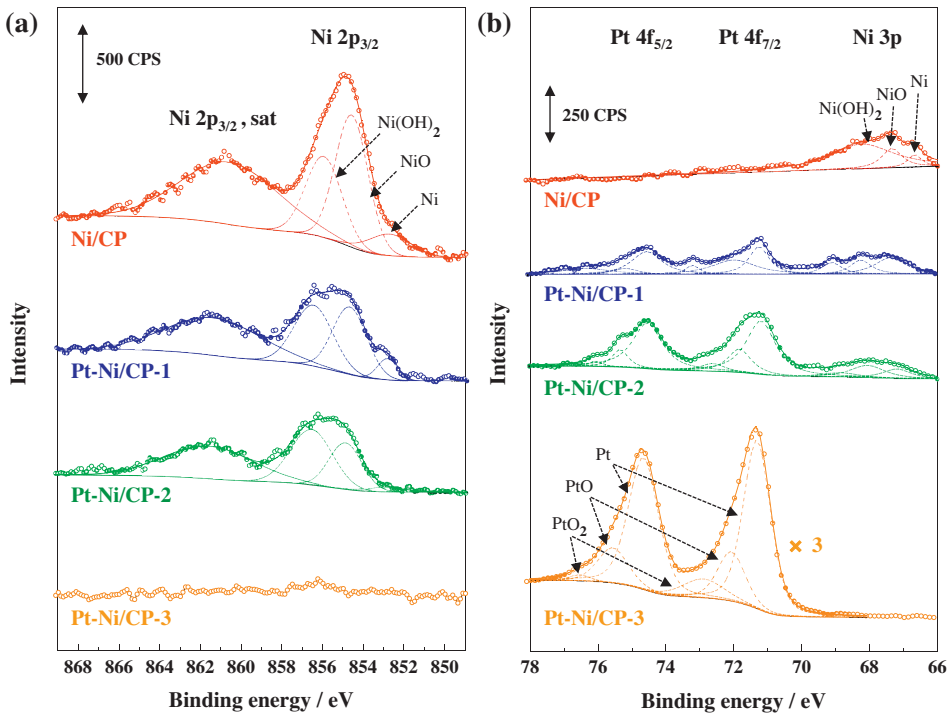

Fig. 5. XPS spectra of Ni/CP and Pt-Ni/CP electrodes. (a) Ni 2p3/2 and (b) Ni 3p + Pt 4f.

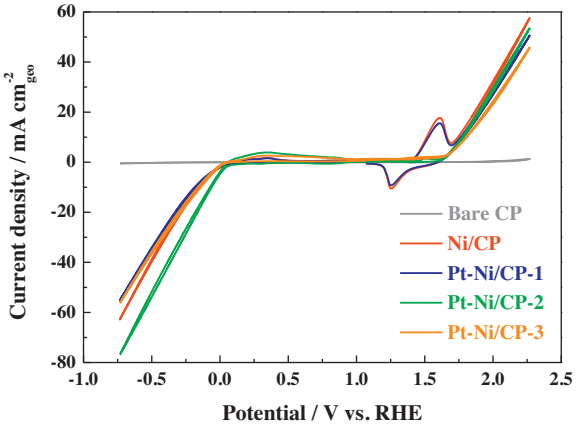

Fig. 6. CV curves of the bare CP, Ni/CP, and Pt-Ni/CP electrodes in 1.0 M KOH with a scan rate of 50 mV s^{-1} at room temperature.

even though the Pt molar concentration was 72.2% based on ICPMS measurement.

Cyclic voltammetry was employed to investigate the electrochemical behavior of the prepared electrodes in a 1.0 M KOH electrolyte as shown in Fig. 6. Bare CP (gray line) showed no activity within the tested potential range. For the Ni/CP electrode, the reduction and oxidation peaks for reversible surface Ni oxidation (β-$Ni(OH)_2 \leftrightarrow$ NiOOH) were clearly observed at 1.25 V_{RHE} and 1.60 V_{RHE}, respectively [27]. As the Pt content increased, the intensity of these redox peaks slightly decreased for Pt-Ni/CP-1 and then completely disappeared for Pt-Ni/CP-2 and Pt-Ni/CP-3 indicating significantly high coverage of the Ni surface by Pt particles, which are corresponded to the surface analysis by XPS (Fig. 5).

Pt-Ni/CP-2 (−73.7 mA cm_{geo}^{-2} at −0.70 V_{RHE}) exhibited highly enhanced HER activities compared to the untreated Ni/CP (−59.4 mA cm_{geo}^{-2}). The improved HER activity of the Pt-Ni/CP-2 electrode can be explained by the moderately uncovered Ni surface providing sufficient water dissociation sites to the Pt particles. In evidence of this, Markovic et al. demonstrated an enhanced activity of Pt for the HER with the formation of H_{ad} intermediates on a Pt surface promoted by neighboring $Ni(OH)_2$ nanoscaled clusters [28,29]. However, an increase in activity was not achieved for Pt-Ni/CP-1 (−52.1 mA cm_{geo}^{-2}) and Pt-Ni/CP-3 (−53.4 mA cm_{geo}^{-2}). This indicates that the synergic interaction between neighboring Pt and Ni atoms was not significant due either to the amount of Pt being too low (Pt-Ni/CP-1) or there being insufficient Ni exposed to water (Pt-Ni/CP-3), whereas the HER activity was affected by the Ni loading decrease during the displacement process. In the case of the OER, the Ni/CP electrode showed the highest activity as Ni is the more active material for the OER in an alkaline solution compared to Pt [30].

Fig. 7a shows the performance of AEMWEs with different HER electrodes. In our previous study, when Ni/CP electrodes were employed as both HER and OER electrodes, the AEMWE cell exhibited a current density of 150 mA cm^{-2} at a cell voltage of 1.9 V and operating temperature of 50 °C [23]. Under identical operating conditions and only changing the HER electrode to Pt-Ni/CP-2, the current density was significantly enhanced to 250 mA cm^{-2} showing a 1.7 times improvement by adding an ultra-low amount of Pt (1.85 μg_{Pt} cm^{-2}). It should also be emphasized that the Ni loading remained extremely low (2.85 μg_{Ni} cm^{-2}). Further enhancement of cell performance was achieved by increasing the cell temperature to 70 °C.

Fig. 7b shows a summary of the reported AEMWE performances described by the current density at a cell voltage of 1.9 V (for more details see Table S1) [11–19,23]. Although the total catalyst loading was about two-orders lower, the current density of the particle-type electrodes in the present study was comparable to or even higher than that reported in the literature using either conventional porous electrodes containing a non-noble catalyst with a loading of 4.5 ~ 5.0 mg cm^{-2} (blue square, open) [11–13] or adding a noble catalyst with a loading of 0.1 ~ 1.0 mg_{Pt} cm^{-2} (blue inverted triangle, half-open) [16,17]. The performance observed in this study was

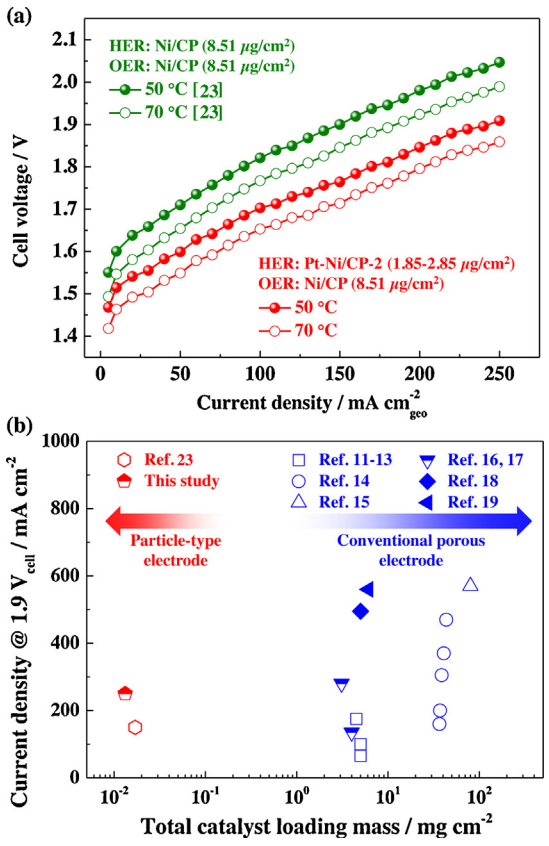

Fig. 7. (a) Effect of the HER electrode on the performance of AEMWE cells. Polarization curves with 1.0 M KOH at a feed rate of 1 mL min^{-1} under operating temperatures of 50 °C and 70 °C [polarization curves in green "reprinted from Reference 23 with permission from Elsevier"]. (b) Recorded current densities of a AEMWE cell at 1.9 V reported in the literature [11–19,23] and in the present study (open: non-noble metal only, half-open: non-noble + noble metals, solid: noble metal only).

lower than those observed for conventional porous electrodes containing either non-noble metals with a loading three-orders higher (43 ~ 80 mg cm^{-2}: blue circle, open) [14,15] or a noble metal with a loading two-orders higher (5.0 or 6.1 mg cm^{-2}: blue solid) [18,19]. Our catalyst is, however, still beneficial in terms of cost. In addition, we believe that a particle-type electrode promotes the emission of trapped hydrogen and oxygen bubbles in AEMWE cells, which is an important factor in achieving high performance [20,21,23].

4. Conclusion

Pt-decorated Ni electrocatalysts were successfully prepared on carbon paper by control of galvanic displacement by Pt on the electrodeposited Ni. Among them, the highly populated Pt dots (~50 nm) were formed on the Ni surface immersed in the 1 mM Pt displacement solution containing the HCl concentration of 50 mM. The Pt-Ni/CP-2 electrode with ultra-low Pt loading of 1.85 μg_{Pt} cm^{-2} demonstrated the highest catalytic activity towards HER in 1.0 M KOH solution, because the moderated uncovered Ni surface provided sufficient water dissociation sites to the Pt dots. In the practical application to AEMWE, the MEA employing Pt-Ni/CP-2 as a HER electrode showed the current density of 250 mA cm^{-2} under operating temperature of 50 °C, and this achievement is 1.7 times enhanced performance, compared with the MEA employing Ni/CP as a HER electrode.

Acknowledgement

This work was supported by the Korean Government through the New & Renewable Energy Core Technology Program of the Korea Institute of Energy Technology Evaluation and Planning (KETEP) funded by MOTIE (No.20133030011320), the Korea CCS R&D Center (KCRC) grant funded by MSIP (No. 2013M1A8A1038315), the National Research Foundation of Korea Grant funded by MSIP (2014, University-Institute cooperation program), the Global Frontier R&D Program on Center for Multiscale Energy System funded by the National Research Foundation, MSIP (No. 2012M3A6A7054283), and the Basic Science Research Program funded by the National Research Foundation of Korea (NRF), MEST (2014R1A1A2057136). This work was also financially supported by KIST through the Institutional Project.

References

[1] K. Christopher, R. Dimitrios, Energy Environ. Sci. 5 (2012) 6640–6651.
[2] K. Zeng, D. Zhang, Prog. Energy Combust. Sci. 36 (2010) 307–326.
[3] A.S. Aricò, S. Siracusano, N. Briguglio, V. Baglio, A.D. Blasi, V. Antonucci, J. Appl. Electrochem. 43 (2013) 107–118.
[4] A. Goñi-Urtiaga, D. Presvytes, K. Scott, Int. J. Hydrogen Energy 37 (2012) 3358–3372.
[5] J.R. Varcoe, P. Atanassov, D.R. Dekel, A.M. Herring, M.A. Hickner, P.A. Kohl, A.R. Kucernak, W.E. Mustain, K. Nijmeijer, K. Scott, T. Xu, L. Zhuang, Energy Environ. Sci. 7 (2014) 3135–3191.
[6] M. Carmo, D. Fritz, J. Mergel, D. Stolten, Int. J. Hydrogen Energy 38 (2013) 4901–4934.
[7] J. Durst, A. Siebel, C. Simon, F. Hasché, J. Herranz, H.A. Gasteiger, Energy Environ. Sci. 7 (2014) 2255–2260.
[8] E. Antolini, ACS Catal. 4 (2014) 1426–1440.
[9] Y. Lee, J. Suntivich, K.J. May, E.E. Perry, Y. Shao-Horn, J. Phys. Chem. Lett. 3 (2012) 399–404.
[10] G. Chen, X. Chen, P.L. Yue, J. Phys. Chem. B 106 (2002) 4364–4369.
[11] Y. Cao, X. Wu, K. Scott, Int. J. Hydrogen Energy 37 (2012) 9524–9528.
[12] X. Wu, K. Scott, J. Power Sources 214 (2012) 124–129.
[13] X. Wu, K. Scott, Int. J. Hydrogen Energy 38 (2013) 3123–3129.
[14] C.C. Pavel, F. Cecconi, C. Emiliani, S. Santiccioli, A. Scaffidi, S. Catanorchi, M. Comotti, Angew. Chem. 126 (2014) 1402–1405.
[15] L. Xiao, S. Zhang, J. Pan, C. Yang, M. He, L. Zhuang, J. Lu, Energy Environ. Sci 5 (2012) (2015) 7869–7871.
[16] X. Wu, K. Scott, J. Mater. Chem. 21 (2011) 12344–12351.
[17] X. Wu, K. Scott, F. Xie, N. Alford, J. Power Sources 246 (2014) 225–231.
[18] J. Parrondo, C.G. Arges, M. Niedzwiecki, E.B. Anderson, K.E. Ayers, V. Ramani, RSC Adv. 4 (2014) 9875–9879.
[19] Y. Leng, G. Chen, A.J. Mendoza, T.B. Tighe, M.A. Hickner, C. Wang, J. Am. Chem. Soc. 134 (2012) 9054–9057.
[20] F. Arbabi, A. Kalantarian, R. Abouatallah, R. Wang, J.S. Wallace, A. Bazylak, J. Power Sources 258 (2014) 142–149.
[21] D. Zhang, K. Zeng, Ind. Eng. Chem. Res. 51 (2012) 13825–13832.
[22] G. Merle, M. Wessling, K. Nijmeijer, J. Membr. Sci. 377 (2011) 1–35.
[23] S.H. Ahn, B. Lee, I. Choi, S.J. Yoo, H. Kim, E. Cho, D. Henkensmeier, S.W. Nam, S. Kim, J.H. Jang, Appl. Catal. B Environ. 154–155 (2014) 197–205.
[24] W. Sheng, M. Myint, J.G. Chen, Y. Yan, Energy Environ. Sci. 6 (2013) 1509–1512.
[25] L. Gan, M. Heggen, S. Rudi, P. Strasser, Nano Lett. 12 (2012) 5423–5430.
[26] S. Papadimitriou, A. Tegou, E. Pavlidou, S. Armyanov, E. Valova, G. Kokkinidis, S. Sotiropoulos, Electrochim. Acta 53 (2008) 6559–6567.
[27] P. Oliva, J. Leonardi, J.F. Laurent, C. Delmas, J.J. Braconnier, M. Figlarz, F. Fievet, A. Guibert, J. Power Sources 8 (1982) 229–255.
[28] R. Subbaraman, D. Tripkovic, D. Strmcnik, K. Chang, M. Uchimura, A.P. Paulikas, V. Stamenkovic, N.M. Markovic, Science 334 (2011) 1256–1260.
[29] R. Subbaraman, D. Tripkovic, K. Chang, D. Strmcnik, A.P. Paulikas, P. Hirunsit, M. Chan, J. Greeley, V. Stamenkovic, N.M. Markovic, Nat. Mater. 11 (2012) 550–557.
[30] M.H. Miles, J. Electroanal. Chem. Interfacial Electrochem. 60 (1975) 89–96.